

Chapter 11

Tropical Cloud Ensembles

11.1 Introduction

As one proceeds from the west coast of a continent, such as California in North America or Morocco in Northwest Africa, towards the near-equatorial oceanic ITCZ, one notes the following transition in the predominant species of tropical clouds: coastal stratus, stratocumulus, fair weather cumulus, towering cumulus and cumulonimbus. This is a typical scenario over the Pacific and Atlantic Oceans of the two hemispheres. The Asian Monsoon carries some of its own cloud features over the Indian Ocean. Figure 11.1 is a collage of cloud types and typical rainfall distributions over the tropics during the northern summer. This identifies precipitation features, such as those from the ITCZ, typhoon, monsoon, and near coastal phenomena. The precipitation illustrated here was estimated from microwave radiances received by the TRMM satellite. A plethora of clouds types abound in the tropics. Dynamics, physics, and microphysics are important interrelated scientific areas for these clouds' life cycles. Modeling of the life cycle of individual clouds and cloud ensembles and representation of the effects of unresolved clouds in large scale environment are areas of importance for tropical meteorology. The ocean, land surface, and planetary boundary layer large scale wind systems and thermal and humidity stratification have a large control over the nature of evolving clouds.

A background in Cloud Physics is necessary for the understanding of different cloud types and their life cycle. Motions on meso-convective space and time scales have a large influence on these life cycles. The problem is further compounded by the need to know aerosol-cloud interactions, cloud radiative interactions, as well as the mutual interactions among cloud microphysics, dynamics, and other physical processes. Clouds seem to organize from the relatively small scales of the sea breeze to large scales, such as the monsoon. Thus there is a coexistence of clouds and the motion fields on many space and time scales. We allude to some of these issues in the chapter on scale interactions.

A widely used measure of convective instability is the Convective Available Potential Energy, or CAPE. CAPE represents the vertically integrated amount of

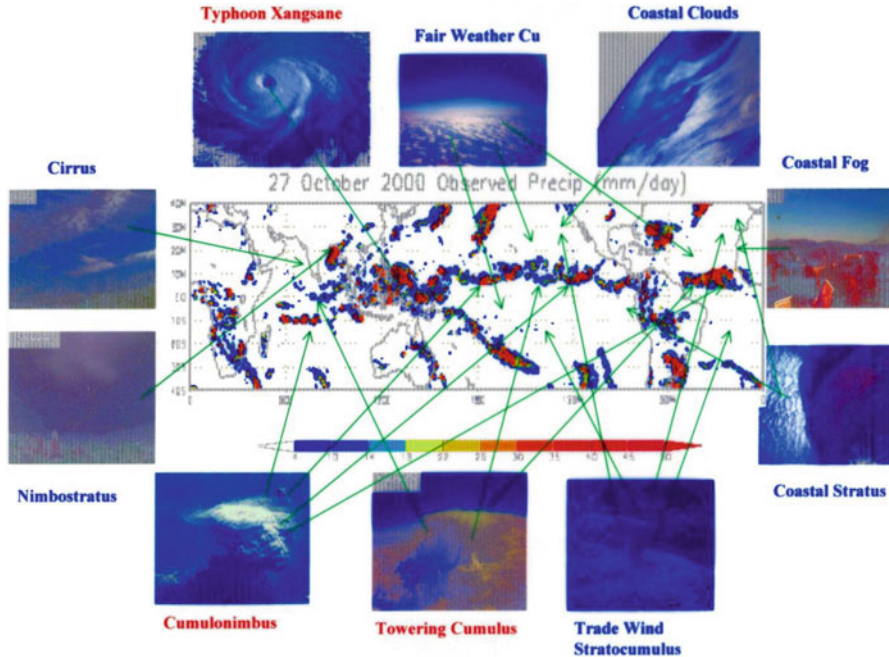


Fig. 11.1 A collage of cloud types and typical rainfall distributions over the tropics during the northern summer

buoyant energy that would be released if a parcel were lifted up to an equilibrium level. It is measured in units of J kg^{-1} . It is usually estimated using a skew-T-log-p diagram. The higher the value of CAPE, the larger the potential for development of deep convection. Negative values of CAPE represent a stable environment. Values of CAPE between 0 and $1,000 \text{ J kg}^{-1}$ are considered marginally unstable; between 1,000 and $2,500 \text{ J kg}^{-1}$ – moderately unstable; between 2,500 and $4,000 \text{ J kg}^{-1}$ – very unstable; and finally, values above $4,000 \text{ J kg}^{-1}$ are considered representative of an extremely unstable atmosphere.

A number of instability measures are important for the understanding of convection. Those can be found in introductory texts on meteorology. The student should be familiar with concepts such as absolute instability, conditional instability, potential instability, etc.

In this chapter we have taken the modeling approach as one that provides some insights on processes that are important for the understanding of buoyancy-driven dry convection, modeling of the non-precipitating shallow stratocumulus and the modeling of cloud ensembles. This approach clearly has its flaws – none of the model examples presented here are perfect. They are based on a number of assumptions and hence have many limitations. Nevertheless, these models are quite useful compared to looking at pictures of clouds and satellite imagery and

gross interpretations that are never very complete in terms of providing insights on the complex interactions we spoke of above. The modeling approach is better suited as an avenue for understanding, provided one is mindful of its limitations.

11.2 Understanding Simple Buoyancy-Driven Dry Convection

Here we shall show an example of a buoyancy-driven cloud model. This model has applications for the understanding of dry convection over warm land surfaces. It describes the growth of a buoyancy-driven cloud element in a neutral sounding, i.e., a sounding with an initial stratification that has a constant potential temperature in the vertical. It is possible to develop a rather simple model on an x - z plane to study the growth of such a cloud using a simplified two dimensional vorticity equation, the first law of thermodynamics and the mass continuity equation.

Dry convection thermals originate over hot surfaces, such as deserts, where the lowest layers of the atmosphere have superadiabatic lapse rates. Driven by the heating above the surface layer, buoyant thermals, also known as buoyancy driven elements, are generated. These buoyancy driven elements act to destroy the superadiabatic lapse rates. In a hydrostatic environment,

$$0 = -\frac{\partial p}{\partial z} - \rho g \quad (11.1)$$

For a buoyant parcel with a density of ρ' the vertical acceleration is given by

$$\frac{dw}{dt} = -\frac{1}{\rho'} \frac{\partial p'}{\partial z} - g \quad (11.2)$$

Assuming continuity of pressure across the buoyant element, i.e., $\frac{\partial p'}{\partial z} = \frac{\partial p}{\partial z}$ and using the equation of state,

$$p = \rho RT \quad (11.3)$$

the vertical equation of motion (11.2) can be written as

$$\frac{dw}{dt} = -g \frac{T' - T}{T}. \quad (11.4)$$

A buoyancy-driven simple cloud model was first developed by Malkus and Witt (1959) and by Nickerson (1965). This elementary model is most illustrative for the

understanding of dry convection. It is a simple two-dimensional model on the zonal plane (x, z) where the velocity components are defined in terms of the stream function ψ as

$$u = \frac{\partial \psi}{\partial z} \quad (11.5)$$

and

$$w = -\frac{\partial \psi}{\partial x}, \quad (11.6)$$

thus ensuring that the continuity equation

$$\frac{\partial u}{\partial x} + \frac{\partial w}{\partial z} = 0 \quad (11.7)$$

is satisfied. The vorticity equation and the first law of thermodynamics in the x - z plane are written by the relations

$$\frac{\partial \eta}{\partial t} = J(\psi, \eta) - g\phi + \nu \nabla^2 \eta \quad (11.8)$$

$$\frac{\partial \phi}{\partial t} = J(\psi, \phi) + \frac{Q}{\theta_0} + \nu \nabla^2 \phi \quad (11.9)$$

Here η is the relative vorticity given by $\eta = \frac{\partial u}{\partial z} - \frac{\partial w}{\partial x} = \nabla^2 \psi$; $\phi = \frac{\theta - \theta_0}{\theta_0}$ is the normalized potential temperature excess of a parcel with a potential temperature θ_0 with respect to the environment θ ; ν is the viscosity coefficient; and Q denotes the diabatic heating which is defined below. Basically, the problem is regarded as a system of two equations and two unknowns, ψ and ϕ . Once ψ is solved for, one can find u and w from (11.5) and (11.6). This problem still needs the definition of the heating Q and the boundary conditions and initial states for ψ and ϕ . The lateral boundary condition for ψ utilizes a mirror image at $x = 0$ and a Neuman boundary condition $\frac{\partial \psi}{\partial x} = 0$ at $x = L$. Over the north and south boundaries ψ is set to zero and ϕ is set to a constant value. An elevated initial potential temperature excess is defined by

$$\theta - \theta_0 = 0.5 \cos \frac{\pi x}{320} \cos^2 \frac{\pi(z - 100)}{400} \quad (11.10)$$

and this excess resides within $0 \leq x \leq 160m$ and $100 \leq z \leq 300m$. The diabatic heating Q is defined by

$$Q = Q_0 \cos \frac{\pi x}{320} \cos^2 \frac{\pi(z - 100)}{40} \quad (11.11)$$

and resides within $0 \leq x \leq 160m$ and $80 \leq z \leq 120m$. This is a continuous heat source at the base of the warm bubble defined by (11.10). It resides above the Earth's surface between 80 and 120 m and defines an initial buoyancy element. The initial vertical stratification is a neutral state ($\theta_0 = \text{const}$). As the system of equations is integrated, the buoyancy element rises and forms a mushroom cloud near $x = 0$. This growth of the buoyant element is very illustrative of the growth of shallow dry convection.

Figure 11.2a–c shows the results of the model cloud growth at 2, 6 and 10 min after the start of the integration. Here the solid lines represent the potential temperature excess (in °C) and the dashed lines represent the stream function (in m^2s^{-1}). This shows that the potential temperature excess grows in the form of a plume and ends up using most of the initial buoyancy. The life time of this buoyant element is roughly 15 min. Also note that, because of the imposed symmetry about $x = 0$, the left half of the cloud (not shown here) is a mirror image of what the right half (shown here), resulting in a mushroom-shaped cloud.

11.3 Understanding Simple Buoyancy-Driven Shallow Moist Convection

11.3.1 A Simple Cloud Model

The simple cloud model following Murray and Anderson (1965) is a simple non-precipitating shallow convection model. It allows for the formation of liquid water in a supersaturated environment, and for the evaporation of liquid water in a non-saturated environment. Fallout of rain is not permitted. The total moisture (liquid water and water vapor) is thus conserved. An outline of this two-dimensional (x - z) cloud model is presented here.

The vorticity equation is expressed by

$$\frac{\partial}{\partial t} \nabla^2 \psi = -J(\psi, \nabla^2 \psi) + \frac{g}{T_M} \frac{\partial T'}{\partial x} + \nu_M \nabla^4 \psi, \text{ i.e.,} \quad (11.12)$$

Local Change of Vorticity = Vorticity Advection + Buoyancy Term + Friction

Here ψ is a stream function in the vertical plane (x, z) where T_M is a mean temperature for the entire domain and is a constant. T' is the departure of the local

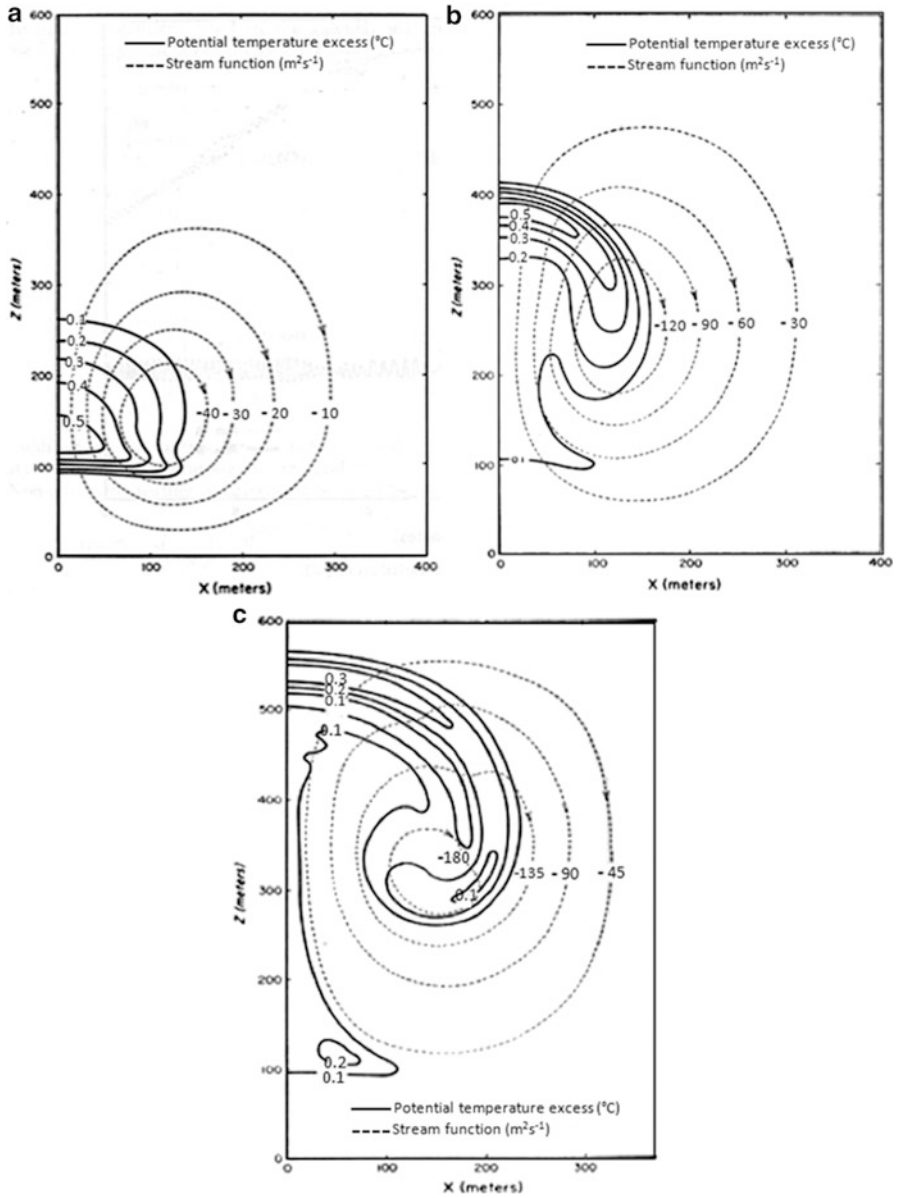


Fig. 11.2 Configuration of the buoyant element at (a) 2, (b) 6, and (c) 10 min after the beginning of integration. Solid lines show the potential temperature excess ($^{\circ}\text{C}$), and dashed lines show the stream function (m^2s^{-1}) (From Nickerson 1965)

temperature T from a horizontal (x) average. ν_M is a diffusion coefficient for the eddy flux of momentum. The stream function is related to the u and w velocity components via the relations

$$\frac{\partial \psi}{\partial z} = u \quad (11.13)$$

and

$$\frac{\partial \psi}{\partial x} = -w, \quad (11.14)$$

so that the continuity equation

$$\frac{\partial u}{\partial x} + \frac{\partial w}{\partial z} = 0 \quad (11.15)$$

is satisfied.

According to (11.12), the buoyancy field ($\frac{\partial T'}{\partial x} > 0$) contributes to vorticity generation, i.e., to $\frac{\partial}{\partial t} \nabla^2 \psi > 0$. This increase in vorticity will, in general, lead to a cellular stream function geometry on the x - z plane with an enhancement of the velocities u and w in different parts of the buoyant cell. This is the mechanism via which buoyancy can initiate motion from an initial state of rest. If T' is locally large and positive, then on either side of it there would be regions of $\frac{\partial T'}{\partial x} > 0$ and $\frac{\partial T'}{\partial x} < 0$ respectively. The rising motion that results in the center will have two sinking lobes on either side.

Any numerical model that is designed to study the time evolution of a phenomenon should have the following ingredients:

- (i) Independent variables;
- (ii) Dependent variables;
- (iii) Closed system of equations
- (iv) Finite differencing schemes for the above;
- (v) Boundary conditions; and
- (vi) Initial conditions.

In this problem, x , z and t are the independent variables. The dependent variables are u , v , ψ , T' , q_l and q_v , where q_l and q_v are, respectively, the specific humidity of liquid water content and that of the water vapor. We need six equations for these six unknowns to close and solve this system. The principal numerical schemes needed for this modeling include a time differencing scheme for marching forward and a Poisson solver to obtain the streamfunction from vorticity. Details on such schemes can be found in texts on numerical methods such as Krishnamurti and Bounoua (1996).

The thermal energy equation is taken as

$$\frac{dT}{dt} = -w \frac{g}{C_p} + \left(\frac{dT}{dt} \right)_{ph} + \nu_T \nabla^2 T, \quad (11.16)$$

where

$$T = T_M + T_0(z) + T'. \quad (11.17)$$

$T_0(z)$ is the initial stratification of temperature of the undisturbed state and is known, and T_M is the (constant) mean domain value. Equation 11.16 describes the change of temperature T from which the changes of T' can be deduced. $\left(\frac{dT}{dt} \right)_{ph}$ is the diabatic change of temperature due to phase change – either condensational heating or evaporative cooling. The changes in liquid water and water vapor respectively arising from phase changes and diffusion may be expressed by:

$$\frac{dq_l}{dt} = \left(\frac{dq_l}{dt} \right)_{ph} + \nu_q \nabla^2 q_l \quad (11.18)$$

$$\frac{dq_v}{dt} = \left(\frac{dq_v}{dt} \right)_{ph} + \nu_q \nabla^2 q_v \quad (11.19)$$

Equations 11.12 through 11.19 constitute a closed system provided the phase change terms are adequately defined. To that end, if $q_v > q_{vs}$, where q_{vs} is the saturation value, the disposition of supersaturation is parameterized from the relation

$$\left(\frac{dq_v}{dt} \right)_{ph} = - \frac{q_v - q_{vs}}{\Delta t} \quad (11.20)$$

Once saturation is reached, the local change for (11.19) is set to zero. Furthermore, one sets

$$\left(\frac{dq_l}{dt} \right)_{ph} = - \left(\frac{dq_v}{dt} \right)_{ph} \quad (11.21)$$

Thus saturation results in removal of water vapor and the formation of an equivalent amount of liquid water.

Liquid water in an unsaturated environment evaporates until the environment is saturated. This is expressed by

$$\left(\frac{dq_l}{dt} \right)_{ph} = - \frac{q_{vs} - q_v}{\Delta t} \quad (11.22)$$

This is the parameterization for the evaporative process. Again, an equivalent increase in water vapor in the water vapor equation is defined by the relation

$$\left(\frac{dq_v}{dt}\right)_{ph} = -\left(\frac{dq_l}{dt}\right)_{ph} \quad (11.23)$$

The condensation heating or evaporative cooling for the thermal equation is next defined by the statement

$$C_p \left(\frac{dT}{dt}\right)_{ph} = -L \left(\frac{dq_v}{dt}\right)_{ph} \quad \text{or} \quad C_p \left(\frac{dT}{dt}\right)_{ph} = +L \left(\frac{dq_l}{dt}\right)_{ph} \quad (11.24)$$

Here one must use the appropriate sign for heating or cooling within the first law of thermodynamics.

The diffusion terms are needed for the suppression of computational waves which could otherwise grow to unrealistic sizes depending on the kind of numerical prediction algorithm one uses. This issue shall not be discussed here.

The system is now closed. The solution procedure involves the following steps:

- (i) An initial buoyancy and an initial state of no motion are specified to start the computation. The initial buoyancy can be in the T' field or it can be introduced via the moisture and thus in the initial horizontal gradient of virtual temperature.
- (ii) The vorticity (11.12) yields a new value of the stream function; this in turn gives the values of u and w from (11.13) and (11.14).
- (iii) The two moisture equations provide new values of q_l and q_v .
- (iv) The thermal (11.24) provide a prediction of the temperature T and thus the temperature deviation T' field

11.3.2 *Initial and Boundary Conditions and Domain Definition*

At $x = 0$, the horizontal gradient $\partial/\partial x$ of all quantities is set to zero, and the stream function is a constant at $z = 0$, $z = z_T$ and $x = x_R$ (the bottom, top and right boundaries of the domain). The perturbation temperature T' vanishes at these boundaries. The liquid water content is set to zero at the boundaries, and is also initially set to zero over the entire domain. Initially there is no horizontal gradient of water vapor q_v and carries an initial vertical stratification. The initial thermal stratification shows a conditional instability for the $T_0(z)$ field in the lower troposphere. A perturbation in the T' field is used to introduce an augmentation of the virtual temperature that supplies the initial buoyancy perturbation necessary for the growth of convection.

The domain is an $8,000 \text{ m} \times 8,000 \text{ m}^2$ within which there are grid points at every 250 m in the x and z directions. In the actual simulations of the cloud Murray and Anderson set $\nu_M = 500 \text{ m}^2 \text{ s}^{-1}$ and $\nu_q = \nu_T = 0$. The time step for calculations is 15 s, which satisfies the linear stability criterion.

11.3.3 Numerical Model Results

Figure 11.3a–d shows the evolution of the equivalent potential temperature θ_e at forecast times of 0, 10, 15, and 20 min from the beginning of integration. The initial state distribution of θ_e has a minimum at the 3 km height. This initial state is conditionally unstable. Near the ground, in the lowest half kilometer, the initial state contains a stable layer. The initial buoyancy perturbation is placed above this surface stable layer to initiate the cloud growth. As time proceeds to 10, 15, and 20 min one sees the growth of the cloud streamfunction and the evolution of the θ_e field. The distortion of the θ_e isopleths by the evolving wind as a function of time is very impressive. This evolution reduces the overall conditional instability over the x - z plane as the cloud grows within it. The x -averaged reduction of the slope of θ_e is illustrated in Fig. 11.4. This shows that a single cloud can substantially reduce the conditional instability of the environment. Counteracting forcings must then come into play in order to restore the conditional instability of the large scale tropics (see Chap. 14).

The time history of vertical velocity and temperature departure at the axis of the cloud ($x = 0$) is shown in Fig. 11.5a, b. These are height-time sections covering the life cycle of the model cloud. Figure 11.5a shows the evolution of the axis-centered vertical velocity w (m s^{-1}) for 40 min of integration. The upward motion starts almost immediately, reaching a maximum value of nearly 13 ms^{-1} at a height of 2.8 km above the ground 14 min after the initial time. After that the cloud dies out by around 24 min. Thereafter mostly weak downward flows prevail. The attendant temperature departure T' (i.e., the warm and cold anomalies with respect to the initial state horizontal average of temperature) is shown in Fig. 11.5b. By around 12 min the latent heating provides a warm anomaly on the order of 5°C at a height of 2.8 km. After 16 min this warm core weakens and narrows to 2°C near the 3 km level.

A very interesting aspect of this cloud model is the buoyancy-induced overshooting of vertical motion. This overshooting of vertical motion above the cloud results in cloud evaporation and adiabatic cooling and a narrow cold cap above the cloud is seen. This cold cap has a temperature anomaly of -4°C and lasts through roughly 28 min of integration.

Figure 11.6a–d shows the corresponding history of the growth of the streamfunction ψ on the x - z plane (solid lines) and of the liquid water mixing ratio (dashed lines) for times 5, 10, 15, and 20 min. The isopleths for the liquid water mixing ratio starting at values $\geq 0.4 \text{ g kg}^{-1}$ outline the shape of the model cloud (generally, visible clouds in the tropics have liquid water mixing ratios in excess of this threshold value). In the first 15 min of this time history one sees the

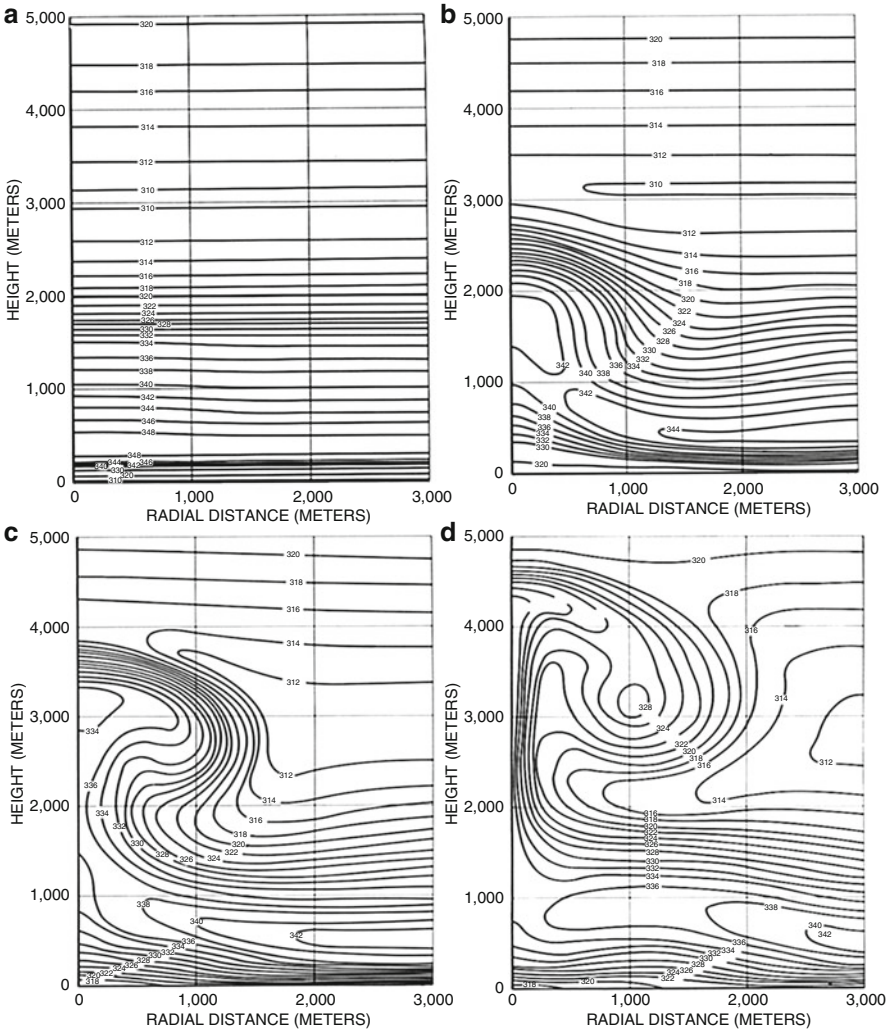


Fig. 11.3 x - z cross-sections of the model potential temperature at time (a) top left 0, (b) top right 10, (c) bottom left 15, and (d) bottom right 20 min illustrating the evolution of the model moist shallow convection (From Murray et al. 1965)

spectacular growth of the model cloud and the associated circulation described by the streamfunction. Thereafter the cloud slowly starts to weaken. However, it remains active near the axis ($x = 0$) at a height of near 3.5 km. At 20 min, the horizontal size of the cloud is around 1 km, and its vertical extent is about 4 km.

These numerical results can be regarded as a simulation of the life cycle of a shallow non-precipitating stratocumulus cloud.

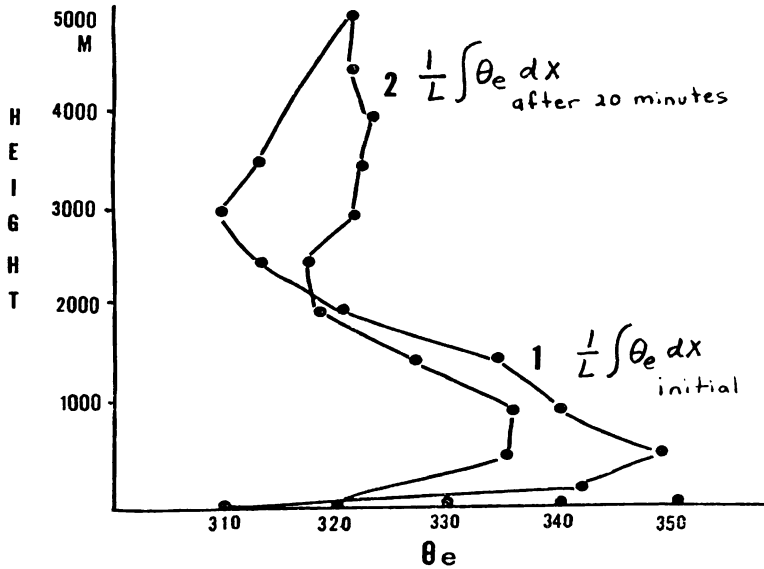


Fig. 11.4 Vertical profiles of horizontally averaged potential temperature at the initial time and 20 min into the integration

11.4 A Cloud Ensemble Model

There are several cloud ensemble models that have been developed in recent years. These models include several forms of water substance, including vapor, liquid and ice phase. In this section we will provide a description of one such model that was developed by Tao and Simpson (1993).

11.4.1 Kinematics and Thermodynamics

The equation of state is given by

$$p = \rho RT(1 + 0.61q_v) \quad (11.25)$$

where p , ρ and T are the pressure, density and temperature of the air, and $(1 + 0.61q_v)$ is the virtual temperature correction for air with specific humidity q_v . In the following equations the Exner pressure π will be used; it is defined as

$$\pi = (p/p_0)^{R/C_p}, \quad (11.26)$$

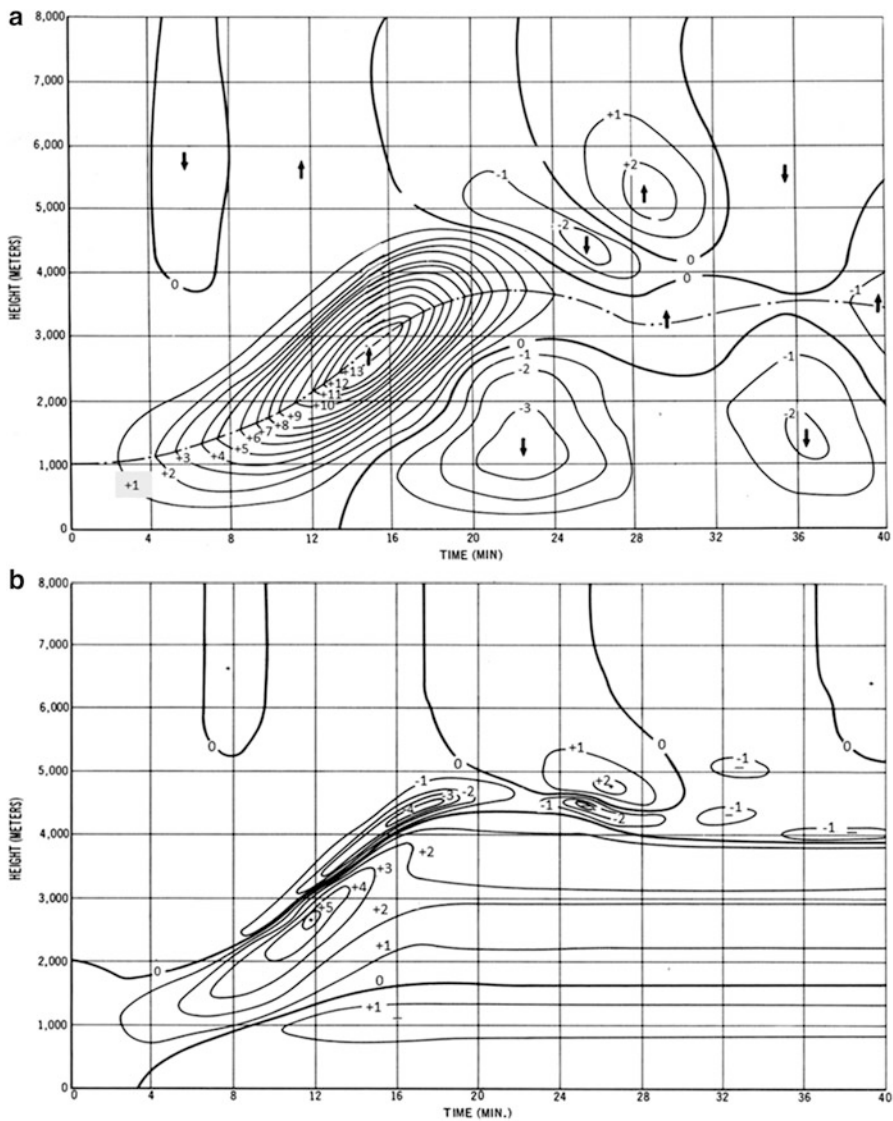


Fig. 11.5 Time-height cross-sections of (a) top vertical velocity, and (b) bottom temperature departure. Centered at $x = 0$ (From Murray and Anderson 1965)

where p_0 is a reference pressure. The virtual potential temperature is defined as

$$\theta_v = \theta(1 + 0.61q_v) \tag{11.27}$$

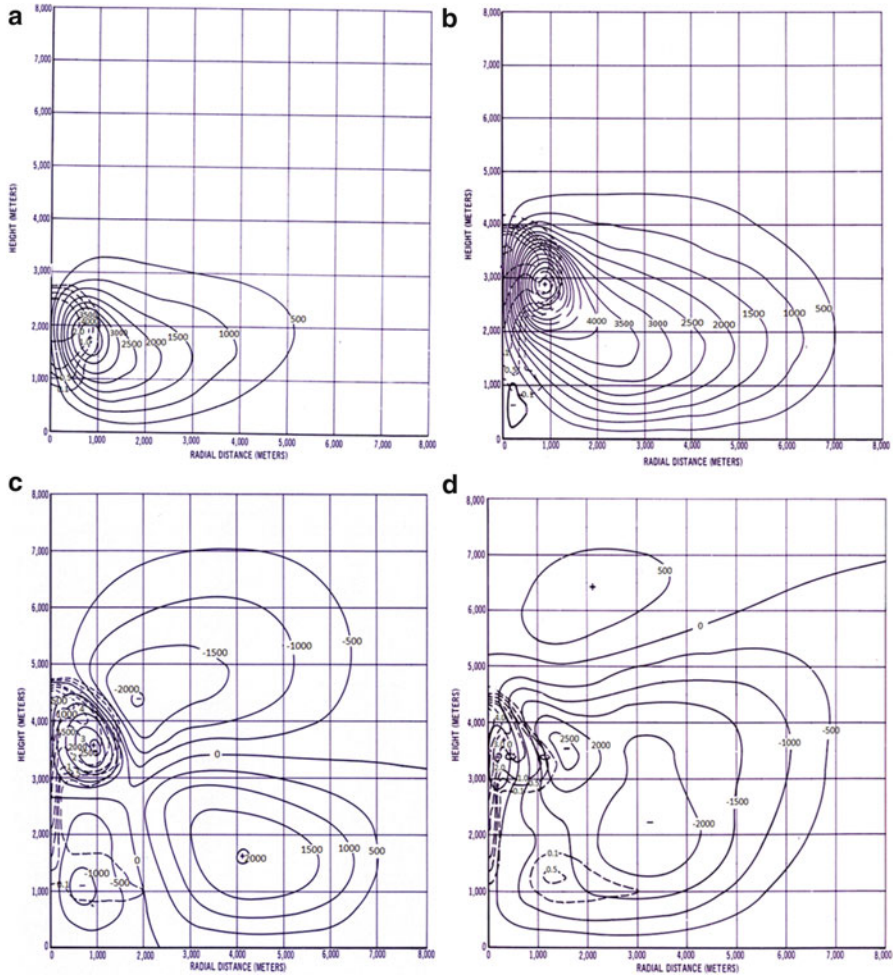


Fig. 11.6 Streamlines (*solid*) and liquid water mixing ratio (*dashed*) at (a) 10, (b) 15, (c) 20 and (d) 25 min (From Murray and Anderson 1965)

Using the definition of potential temperature, $\theta = T(p_0/p)^{R/C_p}$, or in other words, $\theta = T/\pi$, the three equations of motion can be written as:

$$\frac{\partial u}{\partial t} = -\frac{\partial}{\partial x}(uu) - \frac{\partial}{\partial y}(uv) - \frac{1}{\bar{\rho}} \frac{\partial}{\partial z}(\bar{\rho}uw) - C_p \bar{\theta} \frac{\partial \pi'}{\partial x} + fv + D_u \quad (11.28)$$

$$\frac{\partial v}{\partial t} = -\frac{\partial}{\partial x}(uv) - \frac{\partial}{\partial y}(vv) - \frac{1}{\bar{\rho}} \frac{\partial}{\partial z}(\bar{\rho}vw) - C_p \bar{\theta} \frac{\partial \pi'}{\partial y} - fu + D_v \quad (11.29)$$

$$\frac{\partial w}{\partial t} = -\frac{\partial}{\partial x}(uw) - \frac{\partial}{\partial y}(wv) - \frac{1}{\bar{\rho}} \frac{\partial}{\partial z}(\bar{\rho}ww) - C_p \bar{\theta} \frac{\partial \pi'}{\partial z} + g \left(\frac{\theta'}{\bar{\theta}} + 0.61q'_v - q_l \right) + D_w \quad (11.30)$$

In these equations u , v and w are the zonal, meridional and vertical wind components; g is the acceleration of gravity; q_l is the mixing ratio of liquid water plus that of ice. Primes denote departures from the corresponding horizontal area-average. The horizontal area averages in turn are denoted by an overbar. D_u , D_v and D_w are the momentum diffusion rates of the sub-grid scales in the three respective directions. The thermodynamic energy equation is written as

$$\begin{aligned} \frac{\partial \theta}{\partial t} = & -\frac{\partial}{\partial x}(u\theta) - \frac{\partial}{\partial y}(v\theta) - \frac{1}{\bar{\rho}} \frac{\partial}{\partial z}(\bar{\rho}w\theta) + D_\theta \\ & + \frac{L_v}{C_p}(c - e_c - e_r) + \frac{L_f}{C_p}(f_r - m) + \frac{L_s}{C_p}(d - s) + Q_R \end{aligned} \quad (11.31)$$

where L_v , L_f and L_s denote, respectively, the latent heats of condensation, fusion and sublimation; c , e_c , and e_r are the rates of condensation, evaporation of cloud water, and evaporation of cloud droplets respectively; f_r and m are the rates of freezing of raindrops and of melting of snow, graupel or hail; d and s are the rates of deposition and sublimation of ice particles. Q_R is the radiative heating or cooling, and D_θ is the horizontal diffusion rate of potential temperature.

The equation for the specific humidity of water vapor can be written as

$$\frac{\partial q_v}{\partial t} = -\frac{\partial}{\partial x}(uq_v) - \frac{\partial}{\partial y}(vq_v) - \frac{1}{\bar{\rho}} \frac{\partial}{\partial z}(\bar{\rho}wq_v) + D_{q_v} - (c - e_c - e_r) - (d - s) \quad (11.32)$$

Here D_{q_v} is the horizontal diffusion rate for water vapor.

11.4.2 Cloud Microphysics

We will next address the water substance components of the model and their rates of growth. A drop size distribution function $N(D)$ is assumed as

$$N(D) = N_0 e^{-\lambda D}$$

i.e. the number of drops N (per unit volume of space) of a given size D is inversely proportional to that size. N_0 , the value of N at $D = 0$, is called an intercept parameter. λ is called the slope of the particle size distribution and is empirically expressed by

$$\lambda = \left(\frac{\pi \rho_x N_0}{\rho q_x} \right)^{1/4} \quad (11.33)$$

where ρ_x and q_x are the density and mixing ratio of the specific hydrometeor.

The model uses values of the intercept parameter for graupel, snow and rain that are around 0.04, 0.04 and 0.08 cm^{-4} respectively. The densities for graupel, snow and rain are respectively 0.4 g cm^{-3} , 0.1 g cm^{-3} and 1 g cm^{-3} . For cloud ice, the model assumes a single value of size with diameter of 2×10^{-3} cm and a density of 0.917 g cm^{-3} .

The prognostic equations for the components of the water substance include the following:

(a) Cloud water

$$\begin{aligned} \bar{\rho} \frac{\partial q_c}{\partial t} = & -\frac{\partial}{\partial x}(\bar{\rho} u q_c) - \frac{\partial}{\partial y}(\bar{\rho} v q_c) - \frac{\partial}{\partial z}(\bar{\rho} w q_c) + \bar{\rho}(c - e_c) \\ & - T_{qc} + D_{qc} \end{aligned} \quad (11.34)$$

(b) Rain water

$$\begin{aligned} \bar{\rho} \frac{\partial q_r}{\partial t} = & -\frac{\partial}{\partial x}(\bar{\rho} u q_r) - \frac{\partial}{\partial y}(\bar{\rho} v q_r) - \frac{\partial}{\partial z}[\bar{\rho}(w - V_r)q_r] + \bar{\rho}(-e_r + m - f_r) \\ & - T_{qr} + D_{qr} \end{aligned} \quad (11.35)$$

(c) Ice

$$\begin{aligned} \bar{\rho} \frac{\partial q_i}{\partial t} = & -\frac{\partial}{\partial x}(\bar{\rho} u q_i) - \frac{\partial}{\partial y}(\bar{\rho} v q_i) - \frac{\partial}{\partial z}(\bar{\rho} w q_i) + \bar{\rho}(d_i - s_i) \\ & - T_{qi} + D_{qi} \end{aligned} \quad (11.36)$$

(d) Snow

$$\begin{aligned} \bar{\rho} \frac{\partial q_s}{\partial t} = & -\frac{\partial}{\partial x}(\bar{\rho} u q_s) - \frac{\partial}{\partial y}(\bar{\rho} v q_s) - \frac{\partial}{\partial z}[\bar{\rho}(w - V_s)q_s] \\ & + \bar{\rho}(d_s - s_s - m_s + f_s) - T_{qs} + D_{qs} \end{aligned} \quad (11.37)$$

(e) Graupel

$$\begin{aligned} \bar{\rho} \frac{\partial q_g}{\partial t} = & -\frac{\partial}{\partial x}(\bar{\rho} u q_g) - \frac{\partial}{\partial y}(\bar{\rho} v q_g) - \frac{\partial}{\partial z}[\bar{\rho}(w - V_g)q_g] \\ & + \bar{\rho}(d_g - s_g - m_g + f_g) - T_{qg} + D_{qg} \end{aligned} \quad (11.38)$$

On the right hand side of the above equations there are terms of the kind $\bar{\rho}(c - e_c)$, $\bar{\rho}(-e_r + m - f_r)$, $\bar{\rho}(d_i - s_i)$, etc. Taking (11.35) as an example, $\bar{\rho} \frac{\partial q_r}{\partial t} = \dots + \bar{\rho}(-e_r + m - f_r) + \dots$, the right hand side is interpreted as follows – evaporation (e_r) and freezing (f_r) reduce the mixing ratio of rain water q_r ,

therefore they figure in the equation with a minus sign; melting (m) increases the mixing ratio of rain water, therefore it figures in the equation with a plus sign. Similar interpretation applies to the terms of this kind in all the above equations.

The transfer rates among the different hydrometeor species are denoted by T with the relevant subscript. These are expressed by the following equations:

$$T_{qc} = -(P_{sacw} + P_{raut} + P_{racw} + P_{sfw} + D_{gacw} + Q_{sacw}) - P_{ihom} - P_{imlt} - P_{idw} \quad (11.39)$$

$$T_{qi} = -(P_{saut} + P_{saci} + P_{raci} + P_{sfi} + D_{gaci} + W_{gaci}) + P_{ihom} - P_{imlt} + P_{idw} \quad (11.40)$$

$$T_{qr} = Q_{sacw} + P_{raut} + P_{racw} + Q_{gacw} - (P_{iacr} + D_{gacr} + W_{gacr} + P_{sacr} + P_{gfr}) \quad (11.41)$$

$$T_{qs} = P_{saut} + P_{saci} + P_{sacw} + P_{sfw} + P_{sfi} + \delta_3 P_{raci} + \delta_3 P_{iacr} + \delta_2 P_{sacr} - [P_{gacs} + D_{gacs} + W_{gacs} + P_{gaut} + (1 - \delta_2) P_{racs}] \quad (11.42)$$

$$T_{qg} = (1 - \delta_3) P_{raci} + D_{gaci} + W_{gaci} + D_{gacw} + (1 - \delta_3) P_{iacr} + P_{gacs} + D_{gacs} + W_{gacs} + P_{gaut} + (1 - \delta_2) P_{racs} + D_{gacr} + W_{gacr} + (1 - \delta_2) P_{sacr} + P_{gfr} \quad (11.43)$$

In these equations,

$$W_{gacr} = P_{wet} - D_{gacw} - W_{gaci} - W_{gacs}. \quad (11.44)$$

If the temperature is above freezing,

$$\begin{aligned} P_{saut} &= P_{saci} = P_{sacw} = P_{raci} = P_{iacr} = P_{sfi} = P_{sfw} = D_{gacs} = W_{gacs} \\ &= P_{gacs} = D_{gacr} = P_{gwet} = P_{racs} + P_{sacr} = P_{gfr} = P_{gaut} = P_{imlt} = 0, \end{aligned} \quad (11.45)$$

otherwise

$$Q_{sacw} = Q_{gacw} = P_{gacs} = P_{idw} = P_{ihom} = 0 \quad (11.46)$$

The symbols on the right hand sides of the equations for the transfer rates among different hydrometeor species (11.39) through (11.43) and in Eqs. 11.44 and 11.45 represent different processes as explained in Table 11.1 and illustrated schematically in Fig. 11.7. Each of these is explained in greater detail in Lin et. al. (1983) and Tao and Simpson (1993).

Table 11.1 List of acronyms

Symbol	Meaning
P_{depi}	Depositional growth of cloud ice
P_{int}	Initiation of cloud ice
P_{imlt}	Melting of cloud ice to form cloud water
P_{idw}	Depositional growth of cloud ice at the expense of cloud water
P_{ihom}	Homogeneous freezing of cloud water to form cloud ice
P_{iacr}	Accretion of rain by cloud ice; producing snow or graupel depending on the amount of rain
P_{raci}	Accretion of cloud ice by rain; producing snow or graupel depending on the amount of rain
P_{raut}	Autoconversion of cloud water to form rain
P_{racw}	Accretion of cloud water by rain
$P_{revp} (e_r)$	Evaporation of rain
P_{racs}	Accretion of snow by rain; producing graupel if rain or snow exceeds threshold and $T < 273.16$ or rain if $T > 273.16$
$P(Q)_{sacw}$	Accretion of cloud water by snow; producing snow (P_{sacw}) if $T < 273.16$ or rain (Q_{sacw}) if $T > 273.16$
P_{sacr}	Accretion of rain by snow; producing graupel if rain or snow exceeds threshold; if not, produces snow
P_{saci}	Accretion of cloud ice by snow
P_{saut}	Autoconversion (aggregation) of cloud ice to form snow
P_{sfw}	Bergeron process (deposition and rimming) – transfer of cloud water to form snow
P_{sfi}	Bergeron process embryos (cloud ice) used to calculate transfer rate of cloud water to snow (P_{sfw})
$P_{sdep} (d_s)$	Deposition growth of snow
$P_{ssub} (s_s)$	Sublimation of snow
$P_{smlt} (m_s)$	Melting of snow to form rain, $T > 273.16$
P_{wacs}	Accretion of snow by cloud water to form rain, $T > 273.16$
P_{gaut}	Autoconversion (aggregation) of snow to form graupel
$P_{gfr} (f_g)$	Probabilistic freezing of rain to form graupel
$D(Q)_{gacw}$	Accretion of cloud water by graupel
$D(W)_{gaci}$	Accretion of cloud ice by graupel
$D(W)_{gacr}$	Accretion of rain by graupel
$P_{gsub} (s_g)$	Sublimation of graupel
$P_{gmlt} (m_g)$	Melting of graupel to form rain, $T > 273.16$. (In this regime Q_{gacw} is assumed to be shed as rain)
P_{gwet}	Wet growth of graupel; may involve W_{gacs} and W_{gaci} and must include D_{gacw} or W_{gacr} , or both. The amount of W_{gacw} which is not able to freeze is shed to rain

sensitive to the modeled values of these transfer processes. For illustrative purposes, parameterizations for three of these processes are described below.

(a) Autoconversion (cloudwater to rainwater, P_{raut}):

This process consists of transforming the liquid water from cloud droplets to raindrops. Kessler (1969) formulated a simple parameterization of the role of

autoconversion of liquid water from raindrops with water content m (mass/volume) to raindrops with water content M . The autoconversion is formulated as

$$c_1 = \left[\frac{\Delta q_l}{\Delta t} \right]_{auto} = k_a (q_c - q_{cr}) \quad (11.47)$$

and allows autoconversion process to take place only if the cloud water mixing ratio q_c is greater than a critical value q_{cr} . The values of q_{cr} and k_a used by Kessler are $q_{cr} = 0.05 \text{ g kg}^{-1}$ and $k_a = 0.001 \text{ s}^{-1}$

(b) Accretion (cloud water to rainwater, P_{racw}):

The formulation of accretion follows Kessler (1969) and that of terminal velocity follows Srivastava (1967). After the embryonic rainfall droplets have been formed it is assumed that the water content converts into rain following an inverse exponential distribution function (Marshall-Palmer 1948) $N(D) = N_0 e^{-\lambda D}$, where $N(D)$ is the number of raindrops per unit volume of diameter D , and $\lambda = 3.67/D_0$, where D_0 is a threshold smallest diameter for the start of this process.

The cross-sectional area of the raindrop is $\pi D^2/4$ and its terminal velocity is v_{TD} hence the volume swept by this raindrop per unit time is $v_{TD} \rho q_c \pi D^2/4$. The increase of mass of drops at each diameter is given by

$$\left[\frac{\Delta q}{\Delta t} \right]_{acc} = \int_0^{\infty} v_{TD} \rho q_c \frac{\pi D^2}{4} N(D) dD \quad (11.48)$$

Assuming $v_{TD} = 1500 D^{1/2} \text{ cm s}^{-1}$ and integrating for all diameters, the relation used for the computation of accretion process is obtained as an exact solution of the integral above,

$$c_2 = \left[\frac{\Delta q_l}{\Delta t} \right]_{acc} = \frac{1500\pi}{4} N_0 \rho \frac{\Gamma(3.5)}{\lambda^{3.5}} q_c \quad (11.49)$$

The rainwater mixing ratio is defined as

$$q_r = \int_0^{\infty} q_{rD} dD = \int_0^{\infty} N_0 e^{-\lambda D} \left[\pi \frac{D^3}{6} \rho_w \right] dD \quad (11.50)$$

After integrating $q_r = \pi \rho_w N_0 / \lambda^4$, where ρ_w is the density of liquid water, the value of λ is obtained as an exact solution

$$\lambda = \left(\frac{4\pi \rho_w N_0}{q_r} \right)^{1/4} \quad (11.51)$$

Finally, from

$$v_T = \frac{\int_0^{\infty} q_{rD} v_{TD} dD}{\int_0^{\infty} q_{rD} dD} = \frac{\int_0^{\infty} q_{rD} v_{TD} dD}{q_r} \quad (11.52)$$

Substituting from (11.48) one finally obtains the final fall speed of raindrops as

$$v_T = \frac{1}{\pi \rho_w N_0 \lambda^{-4}} \int_0^{\infty} N_0 e^{-\lambda D} \left(\frac{\pi D^3}{6} \right) \rho_w 1500 D^{1/2} dD \quad (11.53)$$

Or, after solving the above integral exactly,

$$v_T = 1500 \Gamma(4.5) / \lambda^{1/2} \Gamma(4) \quad (11.54)$$

(c) Evaporation (cloud water to vapor, P_{revp}):

The evaporation process follows to some extent the format of Murray and Anderson (1965) If the air is saturated the rate of change of the saturation mixing ratio of water vapor is the same as the rate of change of the saturation mixing ratio. On the basis of conservation of equivalent potential temperature under conditions of saturation mixing ratio is

$$\frac{dq_{vs}}{dt} = -Bw \quad (11.55)$$

and

$$B = \frac{1 - \frac{1}{\varepsilon L} (C_p T - L q_{vs})}{L + \frac{C_p R T^2}{L q_{vs} (\varepsilon + q_{vs})}} g \quad (11.56)$$

where $\varepsilon = 0.62195$ is the molecular weight of water vapor/molecular weight of dry air, $L = 2.5 \times 10^6 \text{ J kg}^{-1}$ is the latent heat of evaporation, and $C_p = 1,004 \text{ J kg}^{-1} \text{ K}^{-1}$ is the specific heat capacity of dry air. The amount of local change in the water vapor mixing ratio is then

$$\Delta q_v = -Bw \Delta t \quad (11.57)$$

In the case of upward motion this represents condensation and is accompanied by an equal and opposite change in cloud water mixing ratio and an increase in temperature, i.e.,

$$\Delta q_c = -\Delta q_v \quad (11.58)$$

$$\Delta T = \frac{L}{C_p} \Delta q_c \quad (11.59)$$

In the case of downward motion of saturated air, the same treatment is used. The increase of mixing ratio, however, accompanying this change is done through evaporation of cloud and/or rain. If cloud water is sufficient to accomplish this change, no rainwater is evaporated. If the cloud water is insufficient some rainwater is evaporated until the sum of cloud water and rainwater evaporation is enough to accomplish the change computed in (11.55).

11.4.4 Modeling Results

In this section we will show some results from Tao and Simpson (1993) and McCumber et al. (1991). These results pertain to some aspects of cloud microphysical sensitivity to the passage of a tropical squall line. This squall line propagated from West Africa into the eastern Atlantic Ocean.

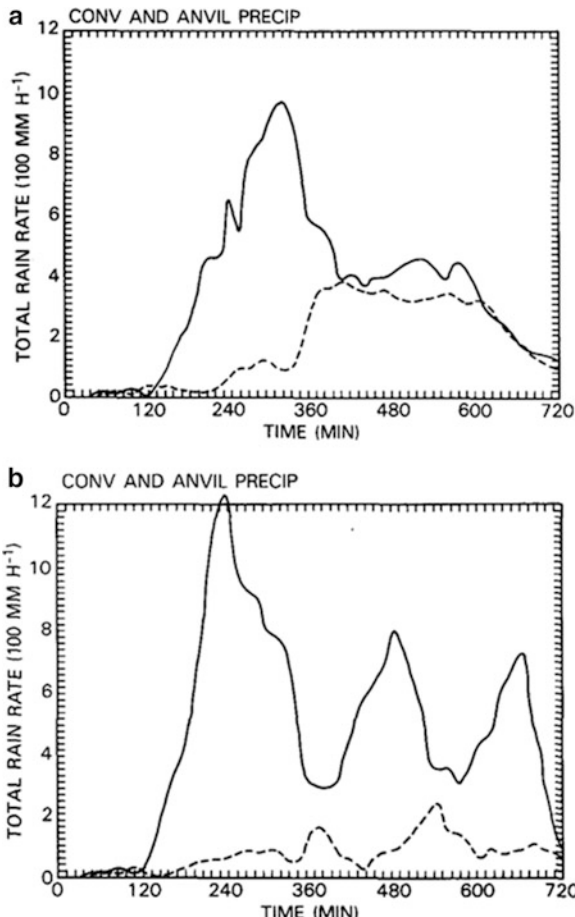
Microphysical sensitivity experiments show some interesting differences from the inclusion versus non inclusion of the ice phase. One of the results was the partitioning of the convective and anvil rain. These results covering a simulated domain of a squall line are shown in Fig. 11.8a, b. When ice phase is excluded the quantitative amount of heavy precipitation increases significantly (and unrealistically). The inclusion of ice brings this heavy precipitation to values that are an order of magnitude smaller and in agreement with observations. The depths of stratiform clouds were considerably reduced when ice was not included (Fig. 11.9a, b). The ice free run lacks a well defined anvil and also carries excessive cellular precipitating towers. This experiment without ice phase also conveyed a slower propagation speed for the squall line.

By using microphysics schemes with varying densities and intercept parameters for the different hydrometeors, one can study the sensitivity of cloud simulations to the distribution and parameterization of hydrometeors.

McCumber et al. (1991) used two experiments with different schemes for modeling the ice phase of water within the cloud. The schemes that he used were:

1. A graupel-only scheme, after Rutledge and Hobbs (1984), which has graupel and snow but no hail processes.
2. A hail-only scheme, after Lin et al. (1983), which has snow and hail but no graupel processes.

Fig. 11.8 Total rain intensity integrated over the grid points designated as the convective and stratiform (anvil) regions from (a) ice run, and (b) ice-free run (Adapted from McCumber et al. 1991)



The main difference between graupel and hail is in the hydrometeors' density – the respective values are 0.4 g cm^{-3} and 0.9 g cm^{-3} – and in their size (graupel particles are generally much smaller).

In the graupel-only case (Fig. 11.10a) the vertical distribution of hydrometeors shows a predominance of graupel over snow particles in the convective and anvil regions. This is a result of the graupel particles being smaller than the snow particles and thus falling more slowly. As a consequence, in the graupel-only case, the melting and deposition of snow are second-order processes. In the hail-only case (Fig. 11.10b), because of the formation and rapid fall out of the hail stones, snow becomes the dominant precipitating hydrometeor within the anvil cloud. This large amount of snow accounts for larger amounts of melting and deposition of snow.

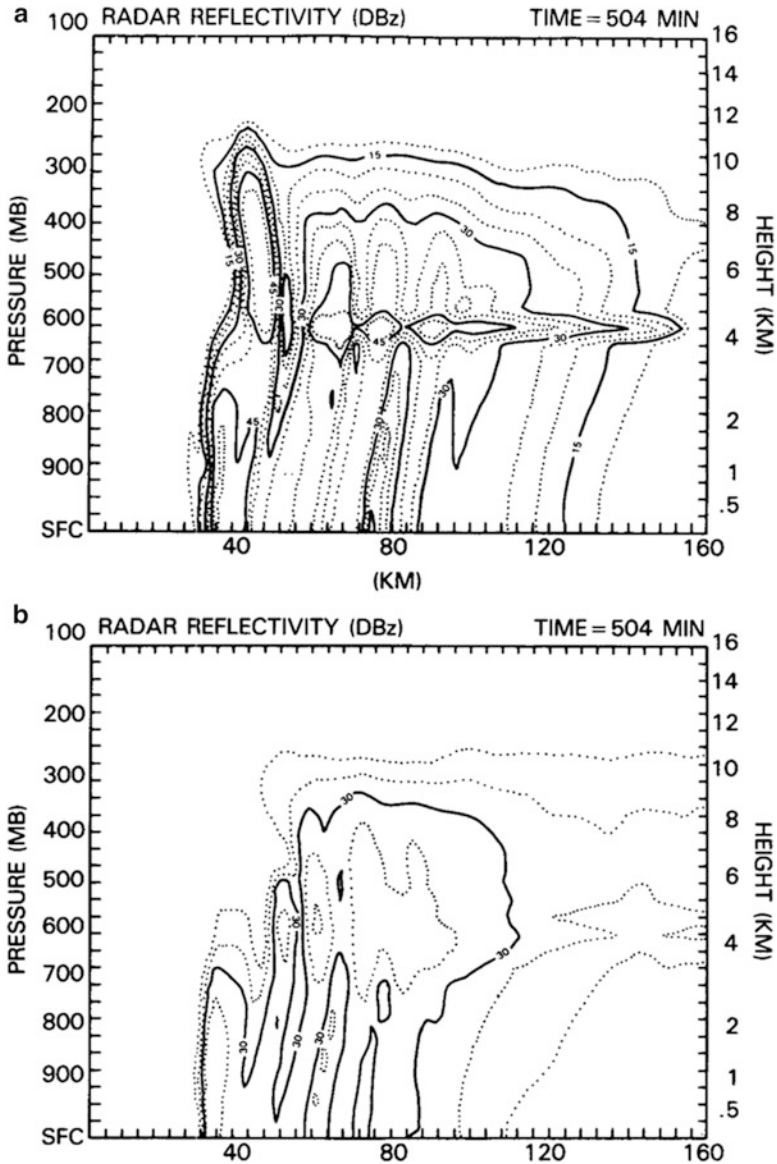


Fig. 11.9 Vertical cross-section of a simulated tropical squall-type convective line at its mature stage from (a) ice run and (b) ice free run. The contour intervals show radar reflectivity at 5dBZ interval beginning from 10dBZ; contours are highlighted at intervals of 15dBZ. From McCumber et al. (1991)

The heating/cooling profiles along the vertical from the above two sensitivity experiments for a tropical squall type convective system are shown in Fig. 11.11b. The hail-only experiment is seen to be characterized by less

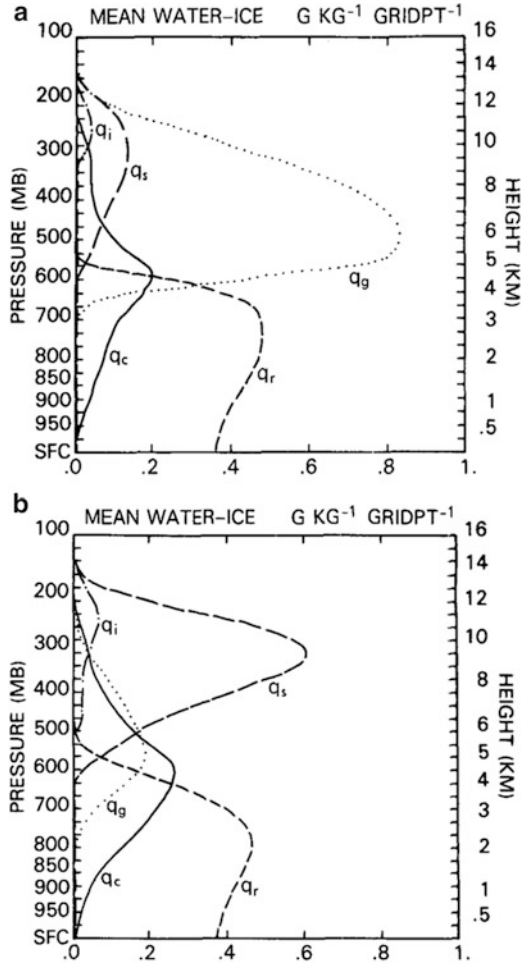
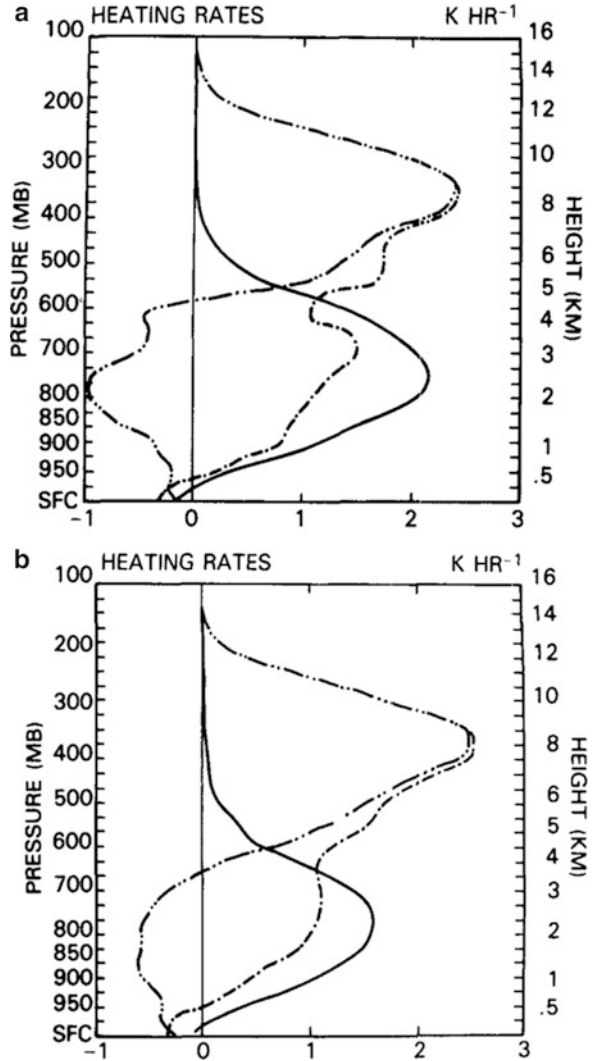


Fig. 11.10 Mean water and ice hydrometeors (g/kg per *grid pint*) depicted as a function of height for tropical squall system simulations. The curves for the hydrometeors shown are rain (qr, *short dash*), cloud water (qc, *solid*), graupel/hail (qg, *dotted*), cloud ice (qi, *dot-dash*), and snow (qs, *long dash*). The units in the figure are normalized with respect to the number of horizontal model grid points. (The unnormalized units are obtained by multiplying by 512 km). The top panel shows results from the graupel-only experiment, while the bottom panel shows results from the hail-only experiment (From McCumber et al. 1991)

diabatic cooling in the lower troposphere compared to the significant cooling in the graupel-only experiment (Fig. 11.11a). The cooling in the hail-only case is mainly attributed to the evaporation of rain and melting of snow (which falls more slowly than hail) and for the graupel-only case there is large scale melting of graupel in the lower troposphere which leads to enhanced lower tropospheric cooling.

Fig. 11.11 Convective heating profiles (K/h) computed for the last 5 h of 2D simulations for tropical squall type convective lines. Shown are the heating in the convective region (*solid*), heating in the anvil region (*double dot-dash*), and the total heating (*dot-dash*). (a) Graupel-only case, and (b) hail-only case (From McCumber et al. 1991)



References

- Kessler, E.: On the distribution and continuity of water substance in atmospheric circulation. Meteor. Monogr. No 32, Amer. Meteor. Soc., 84pp (1969)
- Krishnamurti, T.N., Bounoua, L.: An Introduction to Numerical Weather Prediction Techniques. CRC Press, Boca Raton (1996). 293pp
- Lin, Y.L., Farley, R., Orville, H.D.: Bulk parameterization of the snow field in a cloud model. J. Climate Appl. Meteor. 22, 1065–1092 (1983)
- Malkus, J.S., Witt, G.: The Evolution of a Convective Element: A Numerical Calculation. The Atmosphere and the Sea in Motion, pp. 425–439. The Rockefeller Institute Press, New York (1959)

- Marshall, J.S., Palmer, W.M.K.: The distribution of raindrops with size. *J. Meteor.* **5**, 165–166 (1948)
- McCumber, M., Tao, W.-K., Simpson, J., Penc, R., Soong, S.-T.: Comparison of ice-phase microphysical parameterization schemes using numerical simulations of convection. *J. Appl. Meteor.* **30**, 985–1004 (1991)
- Murray, F.W., Anderson, C.E.: Numerical Simulation of the Evolution of Cumulus Towers, *Report SM-49230*, Douglas Aircraft Company, Inc., Santa Monica, 97pp (1965)
- Nickerson, E.C.: A numerical experiment in buoyant convection involving the use of a heat source. *J. Atmos. Sci.* **22**, 412–418 (1965)
- Rutledge, S.A., Hobbs, P.V.: The mesoscale and microscale structure and organization of clouds and precipitation in mid-latitude clouds. Part XII: a diagnostic modeling study of precipitation development in narrow cold frontal rainbands. *J. Atmos. Sci.* **41**, 2949–2972 (1984)
- Srivastava, R.C.: A study of the effects of precipitation on cumulus dynamics. *J. Atmos. Sci.* **24**, 36–45 (1967)
- Tao, W.-K., Simpson, J.: The Goddard Cumulus ensemble model. Part I: model description. *Terr. Atmos. Oceanic Sci.* **4**, 19–54 (1993)